separations

MDPI

Article

Treatment of Licorice Wastewater via Coagulation–Flocculation and Ozonation Combination: ANN-GA Modeling and Optimization

Babak Rouhi Broujeni [1,*] and Ayoub Karimi-Jashni [2]

[1] Head of Research & Innovation Centre, City University Qatar, Lusail 200197, Qatar
[2] Department of Civil and Environmental Engineering, Shiraz University, Shiraz 71348-51156, Iran; akarimi@shirazu.ac.ir
* Correspondence: babak.rouhibroujeni@cuq-ulster.edu.qa; Tel.: +974-40-198-254

Abstract

This study aimed to remove licorice (Glycyrrhiza glabra) extract from pharmaceutical wastewater using a combination of treatment processes. An Artificial Neural Network (ANN) was coupled with a Genetic Algorithm (GA) to optimize the treatment parameters. Alum, polyaluminum chloride (PAC), and ferric chloride (FC), were first screened for chemical oxygen demand (COD) and color removal, after which alum was selected as the most effective coagulant for further experiments. The optimal ANN structure was identified based on three criteria: mean absolute percentage error, normalized root mean squared error, and correlation coefficient (R). The variables analyzed included pH (7–12), coagulant dose (200–1000 mg L^{-1}), and oxidation time (6–60 min). ANOVA results revealed that coagulant type was the most statistically significant factor influencing both COD and color removal ($p < 0.01$), while pH and dose had relatively lower effects unless paired optimally. Results demonstrated a removal efficiency of approximately 98% under optimal conditions (pH = 10, coagulant dose = 610 mg L^{-1}, and ozonation time = 53 min), with a remaining COD of 190 mg L^{-1}. Overall, the combined coagulation–flocculation and ozonation process demonstrated high effectiveness for the treatment of licorice-based pharmaceutical wastewater.

Keywords: coagulation–flocculation; ozone oxidation; Artificial Neural Network; Genetic Algorithm

Check for updates

Academic Editors: Shaoping Tong and Mingheng Li

Received: 21 July 2026
Revised: 17 August 2026
Accepted: 28 August 2026
Published: 10 September 2026

Copyright: © 2026 by the authors. Licensee MDPI, Basel, Switzerland. This article is an open access article distributed under the terms and conditions of the Creative Commons Attribution (CC BY) license.

1. Introduction

Licorice extract, derived from the roots of Glycyrrhiza glabra, is a valuable ingredient in various industries due to its sweetening, flavoring, pharmaceutical and medicinal properties [1,2]. Estimates suggest licorice extract production reached 40,000–50,000 tonnes over the past decades [3,4]. In most extraction methodologies, the roots of the licorice plant are cleaned, coarsely ground, extracted with boiling water, and then occasionally pressurized [5], followed by subsequent steps of purification or decantation, and then evaporation to achieve the desired moisture content [6]. The extraction process, however, generates a significant amount of wastewater that poses environmental challenges [7,8]. This wastewater is distinguished by high levels of organic matter, color, and suspended solids, posing a threat to receiving environments if left untreated [9,10].

The high chemical oxygen demand (COD) levels with low biodegradability, combined with the presence of phenolic compounds that inhibit bacterial activity and a BOD/COD

ratio often below 0.5, pose challenges to the use of anaerobic and aerobic treatment for licorice-processing wastewater. Ramaswami and colleagues reported that anaerobic digestion achieved only a 15% reduction in COD [4]. Other approaches, including traditional biological technologies, membrane bioreactors, integrated anaerobic–aerobic systems, and advanced oxidation processes have also been attempted to treat high-strength and licorice-processing wastewater [11–15]. Physicochemical treatment methods such as chemical coagulation (CC) and flocculation are extensively employed in the industry to decrease color and turbidity, thereby making the treated effluent more suitable for subsequent secondary biological treatment [16,17]. While biological technologies are cost-effective, their effluent often retains high levels of color, turbidity, and refractory organic compounds. Consequently, conventional treatment processes may not be sufficient for effectively handling this complex wastewater composition. Therefore, there is a critical need to develop efficient and sustainable treatment strategies for licorice-processing wastewater.

Numerous parameters, such as the type of coagulant, pH, and time, can significantly affect coagulation–flocculation and oxidation processes [18–23]. Among these, pH plays a pivotal role, as it directly affects the surface charge of colloidal particles and the speciation of coagulants, ultimately influencing floc formation and pollutant removal [24]. Different coagulants behave optimally at different pH ranges, for instance, alum demonstrates superior performance in near-neutral to slightly alkaline conditions due to the formation of sweep flocs that enhance the entrapment of pollutants [25]. The choice and dose of coagulant are also critical; an optimal dose ensures maximum pollutant removal while avoiding re-stabilization of particles or excess sludge production, which could hinder sedimentation [26]. Recent comparative studies on coagulation combined with oxidation or adsorption such as coagulation–Fenton, coagulation–UV/Persulfate, and coagulation–adsorption have revealed that hybrid processes can substantially improve treatment efficiency, especially in complex wastewaters like those from the textile or chemical industries [27–29]. Although such methods have been widely explored in other industrial wastewaters, further investigation is needed to fine-tune process conditions for specific waste streams such as licorice-based pharmaceutical effluents; consequently, determining optimal parameters is crucial to maximizing efficiency.

Coagulation–flocculation remains an important pretreatment option for highly loaded industrial wastewater because it can effectively remove suspended solids, colloidal matter, a portion of dissolved organic compounds, and color-causing substances through charge neutralization, adsorption, and sweep flocculation [30]. The selection of coagulant is a critical factor because different metal salts exhibit different hydrolysis behaviors, floc characteristics, sludge production tendencies, and pH sensitivities. Among the operational variables, pH plays a particularly important role because it governs metal speciation, surface charge neutralization, and the formation of insoluble hydroxide precipitates, all of which directly influence pollutant removal [31]. For this reason, coagulant selection and pH optimization are essential when designing coagulation-based treatment strategies for complex industrial effluents such as licorice-processing wastewater.

Artificial Neural Networks (ANNs) offer a robust alternative for modeling non-linear systems by approximating experimental regions [32–34]. Recent advancements in artificial intelligence methods, particularly ANNs, have proven highly effective in predicting linear and non-linear process behaviors by analyzing the impact of wastewater treatment parameters on output functions [35,36]. Nodes, or neurons, within the ANN store and process input data to generate output data, using transfer functions to process input signals and influence subsequent layers until the final output is produced [37]. This methodology provides a rapid and straightforward means of predicting various processes compared to complex physical models. Combining ANNs with Genetic Algorithms (GAs) enhances modeling, optimization, and problem-solving capabilities [38–40].

Although licorice-processing wastewater has been examined in a limited number of previous studies, the available literature still provides insufficient information on the performance of sequential coagulation–flocculation and ozonation for simultaneous COD and color removal from real licorice-based pharmaceutical effluent. In particular, the combined effect of coagulant selection, pH adjustment, and ozonation time has not been adequately clarified for this specific wastewater, and the use of data-driven optimization tools for this treatment sequence remains limited. Therefore, the objective of the present study was to evaluate the treatment of highly polluted licorice wastewater through a sequential coagulation–flocculation and ozone-oxidation process. Three coagulants were first screened to identify the most effective option, after which the effects of pH, coagulant dose, and ozonation time were investigated. In addition, a multi-output ANN was developed to predict residual COD and residual color, and GA was applied to identify the optimum operating conditions because the interactions among the selected operating parameters are difficult to describe accurately using simple linear models or one-factor-at-a-time interpretation. This work is intended as a lab-scale feasibility and optimization study for the treatment of licorice-processing wastewater.

2. Materials and Methods

2.1. Experimental Procedure

In this research, wastewater samples were collected from the main wastewater tank of the Shirin-Daru factory, located in Shiraz, Iran. Wastewater was collected by repeated grab sampling from the main wastewater storage tank of the Shirin-Daru factory at different times over approximately one year. Approximately 20 L was collected during each sampling event, immediately refrigerated, and used for experiments as soon as possible. Wastewater characteristics remained relatively stable throughout the sampling period, consistent with the factory's stable production process. The initial characteristics of wastewater are presented in Table 1. Coagulant materials utilized in the study included alum $Al_2(SO_4)_3$ (Al), polyaluminum chloride $Al_2(OH)_nCl_{6-n}$ (PAC), and ferric chloride $FeCl_3$ (FC), all manufactured by Merck. To adjust the pH of the samples, caustic soda and calcium hydroxide were employed. The experimental batch setup included a jar-test device (ET 750, Tintometer GmbH, Dortmund, Germany) for coagulation and flocculation tests. For sample digestion, a DRB200 digestion reactor (Hach Company, Loveland, CO, USA) was utilized, and a DR5000 spectrophotometer (Hach Company, Loveland, CO, USA) was employed to investigate the absorbance of the samples. Concurrently, a HACH 2100P turbidimeter (Hach Company, Loveland, CO, USA) was used for turbidity measurements. Furthermore, a LAB2B ozone generator (Ozonia, Dübendorf, Switzerland) was utilized for the ozone-oxidation step. All experiments were conducted using the batch method and followed the Standard Methods 20th ed., [41].

Phase I: Evaluation of the coagulants

Three coagulants—Al, PAC, and FC—were evaluated for their ability to remove COD and color from the wastewater. Jar-test experiments were carried out using 500 mL of wastewater in each beaker. The initial pH was adjusted using caustic soda and calcium hydroxide prior to coagulant addition [42]. Coagulant doses in the range of 100–1200 mg L^{-1} were tested to determine the suitable dosage range and to identify the most effective coagulant for the subsequent oxidation experiments. Coagulant doses were applied as salt/product doses and, where the chemical composition was defined, were also converted to metal-equivalent doses. The Al-equivalent dose for alum was calculated based on $Al_2(SO_4)_3$, and the Fe-equivalent dose for ferric chloride was calculated based on $FeCl_3$. For PAC, the applied product dose is reported because the aluminum content depends on the specific product composition and basicity. Moreover, the coagulation–flocculation procedure consisted of mixing at 150 rpm for 1 min, followed by mixing at 40 rpm for 20 min, and then settling

for 30 min. All wastewater characterization measurements and treatment experiments were performed independently at least three times. For the characterization of the raw wastewater, 20 measurements were available depending on the parameter, and the results are reported as mean ± SD. No polyelectrolyte was used in this study. The selected operating conditions were adopted based on preliminary tests and standard jar-test practice.

Table 1. Characterization of raw wastewater.

Parameters	Unit	Amount
pH	-	7.35 ± 0.11
COD	mg L^{-1}	10,311 ± 407
BOD	mg L^{-1}	4026 ± 29
TOC	mg L^{-1}	3160 ± 14
Turbidity	NTU	749.8 ± 12.1
Color	mg Pt-CoL^{-1}	1057.5 ± 23.8
TDS	mg L^{-1}	8914 ± 30
TSS	mg L^{-1}	745.4 ± 17.2
Glycyrrhizic acid *	mg L^{-1}	138 ± 5.4

* The glycyrrhizic acid concentration represents an approximate analytical estimate. Owing to the complex wastewater matrix and the presence of multiple organic compounds and process additives, potential analytical interference could not be completely excluded; therefore, this value should be interpreted as indicative rather than as a fully validated quantitative concentration.

Phase II: Oxidation process following coagulation and flocculation

The coagulation–flocculation and ozonation processes were applied sequentially rather than in parallel. After completion of the coagulation–flocculation step and the settling period, the clarified supernatant was withdrawn and transferred to the ozonation reactor for the second treatment stage. This configuration was selected to first reduce the particulate and coagulated pollutant fraction and then apply ozone oxidation to the remaining dissolved organic and color-causing compounds. About 0.8 L of the effluent from the previous treatment step were added to a bottle for ozone-based processes. Ozone was generated from oxygen using a laboratory-scale corona-discharge ozone generator. The generated O_3/O_2 gas stream was introduced into the reactor through a fine-bubble diffuser positioned at the bottom of the reactor. The reactor was continuously fed with an O_2 gas stream using a diffuser positioned at the reactor's base with a concentration of 5 mg L^{-1} ozone. The gas flow rate was maintained at 10 L min^{-1}. The pH of the wastewater was adjusted using NaOH and HCl before ozonation, and the ozonation time was varied according to the experimental design. To prevent any pH change caused by the formation of carboxylic acids, experiments conducted in ultrapure water were buffered to a constant pH. The ozone concentration was controlled based on the ozone generator calibration and the fixed gas-flow setting. Therefore, the reported ozone concentration represents the applied inlet ozone concentration rather than the actual dissolved or consumed ozone concentration. The applied ozone dose was calculated from the inlet ozone concentration, gas flow rate, and reaction time. Residual ozone in the off-gas was not continuously monitored in the present setup; therefore, complete ozone transfer into the liquid phase was not assumed, and the exact consumed ozone dose could not be calculated. For safety, the off-gas was discharged through an ozone destructor before release. The removal percentage of responses was calculated via Equation (1).

$$Removal\% = \frac{C_{Initial} - C_{Final}}{C_{Initial}} \times 100 \quad (1)$$

where $C_{Initial}$ and C_{Final} represent the primary and remaining COD or color values, respectively, which are converted to removal percentages using Equation (1).

The selected experimental ranges for coagulant dose, pH, and ozonation time were chosen based on a combination of preliminary screening tests, physicochemical considerations, and reports from the literature on similar industrial wastewaters. The coagulant

dose range was selected to capture the transition from insufficient destabilization at low dose to possible overdosing effects at high dose. The pH range of 7–12 was chosen to examine the influence of alkaline conditions on both coagulation behavior and ozone-based oxidation. The ozonation time range of 6–60 min was selected to evaluate both the initial rapid oxidation stage and the possible plateau in removal efficiency at longer contact times. These three factors were selected because they are key adjustable operating parameters in the combined coagulation–flocculation and ozonation (CF-OZ) process, while other conditions such as mixing speed, settling time, ozone inlet concentration, gas flow rate, and reactor configuration were kept constant to limit experimental complexity.

2.2. Statistical Analysis

Analysis of variance (ANOVA) was used to evaluate the statistical significance of the investigated factors on COD and color removal. The analysis was performed separately for COD removal and color removal. A significance level of $p < 0.05$ was used to identify statistically significant effects. Degrees of freedom were calculated based on the number of levels for each factor using df = k − 1, where k is the number of factor levels. Replicate measurements were included where available, and average values were used for graphical presentation. Because the experimental program was conducted sequentially rather than as a complete full-factorial design, interaction effects were interpreted only where supported by the available experimental combinations. To evaluate the significance of the variables influencing the responses, the ANOVA was performed using Minitab 16.

2.3. ANN Modeling; Structure and Optimization

ANNs are advanced computational methods that mimic the biological neural networks of the human brain to solve complex problems [43]. The feed-forward architecture of ANNs, specifically the Multilayer Perceptron (MLP), is widely used across various fields for tasks such as prediction, data regression, and analysis [43]. An MLP model consists of multiple layers of highly interconnected computational units (neurons). Each neuron in the hidden layer is interconnected with neurons in both the input and output layers via weighted links, which denote the strength of these connections.

In this study, a dataset comprising dose, pH, and ozonation time as input variables, along with residual COD and residual color as output responses, was used to train the ANN model. The objective was to optimize the neural network architecture for the best predictive performance. The model's performance was evaluated using various metrics, including performance plots, residual plots, and error histograms [44]. Additionally, the mean square error (MSE) and the coefficient of determination (R^2) were calculated upon the completion of each training cycle to assess the model's fit quality with the experimental data.

After determining the best structure of the MLP network for predicting residual COD and residual color, the trained ANN was coupled with a multi-objective Genetic Algorithm (GA) in MATLAB R2025b (Version 25.2) using the gamultiobj function to optimize the operating parameters. The decision variables were pH, alum dose, and ozonation time, while the two separate objective functions were the ANN-predicted residual COD and residual color, which were minimized simultaneously. The optimization was restricted to the experimental domain of pH 7–12, alum dose 200–1000 mg L^{-1}, and ozonation time 6–60 min, and no extrapolation beyond these ranges was permitted. The default gamultiobj algorithm settings were retained, including a population size of 50 and tournament selection. No custom selection, crossover, mutation, or stopping parameters were specified. The multi-objective optimization generated a set of Pareto-optimal candidate operating conditions. From these solutions, the operating scenario providing the highest simultaneous removal of both COD and color was selected as the preferred optimum condition.

$$\text{Objective Function} = \text{Minimize}(\sum_{j=1}^{n_h^*} f^* \left(\left(\sum_1^3 w_{ji} x_i\right) + b_j\right) \times w_{2j}) + \text{b} \quad (2)$$

where x_i represents the independent variables, and w_{ji} and w_{2j} signify the weights of the nodes in the hidden and output layers of the optimized MLP network, respectively. The functions f^* and n^*_h denote the optimal activation function and the number of neurons in the hidden layer, respectively, while also expressing the biases of the nodes in both the hidden and output layers.

To evaluate the predictive performance of the MLP model, the correlation coefficient (R), mean absolute percentage error (MAPE), normalized root mean squared error (NRMSE), and mean squared error (MSE) were calculated using Equations (3)–(6).

$$R = \frac{\sum_{i=1}^{n} (P_{obs,i} - \overline{P}_{obs})(P_{sim,i} - \overline{P}_{sim})}{\sqrt{\sum_{i=1}^{n} (P_{obs,i} - \overline{P}_{obs})^2} \sqrt{\sum_{i=1}^{n} (P_{sim,i} - \overline{P}_{sim})^2}} \quad (3)$$

$$MAPE = \frac{1}{n} \sum_{i=1}^{n} \left| \frac{P_{sim,i} - P_{obs,i}}{P_{obs,i}} \right| \quad (4)$$

$$NRMSE = \sqrt{\frac{\sum_{i=1}^{n} (P_{sim,i} - P_{obs,i})^2}{\sum_{i=1}^{n} (P_{obs,i})^2}} \quad (5)$$

$$MSE = \frac{1}{n} \sum_{i=1}^{n} (P_{sim,\,i} - P_{obs,i})^2 \quad (6)$$

where $P_{sim,i}$ and $P_{obs,i}$ are the simulated and observed values of the response for the ith observation, respectively; $\overline{P}_{sim}$ and $\overline{P}_{obs}$ are their corresponding mean values; and is the total number of observations. The model is considered proficient if its R-value is close to one and the error statistics are nearly zero. A two-tailed t-test was used to statistically compare the two dependent means. The p-value below 0.05 was regarded as indicating statistical significance. The overall workflow used for ANN modeling and GA-based optimization is illustrated in Figure 1.

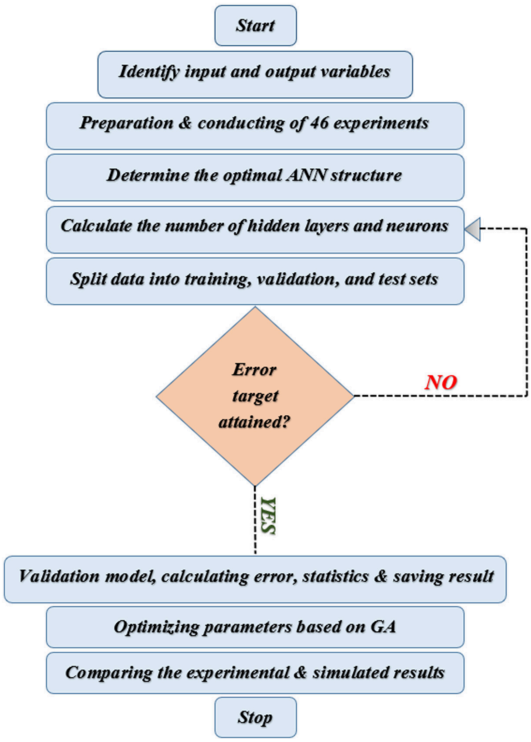


Figure 1. Flowchart for modeling and optimizing COD and color removal.

3. Results and Discussion

3.1. ANOVA Analysis of the Variables

The first set of ANOVA results (Table 2) focused on the effect of coagulant type and dosage on COD removal under a fixed pH condition (pH = 7.1). The analysis revealed that the type of coagulant had a statistically significant impact on COD reduction, with an F-ratio of 6.95, exceeding the critical value ($F_{0.95}$ = 3.49, p = 0.001). In contrast, the coagulant dose yielded an F-ratio of 2.31, below the significance threshold ($F_{0.95}$ = 2.77), indicating its effect was not statistically significant (p = 0.087).

Table 2. ANOVA results for evaluating the significance of coagulant type and dose on COD at fixed pH.

SV [1]	SS [2]	Df [3]	MS [4]	F-Ratio	$F_{0.95}$	SL [5]
Coagulant Type	16,147,304	2	8,073,652	10.43	3.49	0.001
Error	15,487,720	20	774,386			
Total	31,635,024	22				
Coagulant Dose	12,376,628	5	2,475,326	2.31	2.77	0.087
Error	19,258,397	18	1,069,911			
Total	31,635,025	23				

[1] Source of Variation; [2] Sum of Square; [3] Degrees of Freedom; [4] Mean Square; [5] Significance Level.

To explore this further, the influence of pH and coagulant type at optimal dosage conditions was analyzed (Table 3). The results showed that the coagulant type remained the dominant factor, with a remarkably high F-ratio of 76.19 (p < 0.001), while the effect of pH was statistically insignificant (F = 0.29, p = 0.911). These findings clearly demonstrate that coagulant selection plays a critical role in COD removal, more so than the specific pH or the amount of coagulant used when within a reasonable range.

Table 3. ANOVA, the significance of coagulant type and pH on COD (at optimal coagulant concentration).

SV [1]	SS [2]	Df [3]	MS [4]	F-Ratio	$F_{0.95}$	SL [5]
Coagulant (optimal concentration)	32,060,947	2	16,030,473.5	76.19	3.49	<0.001
Error	4,207,799	20	210,389.95			
Total	36,268,746	22				
pH	2,727,721	5	545,544.2	0.293	2.77	0.911
Error	33,541,025	18	1,863,390.28			
Total	36,268,746	23				

[1] Source of Variation; [2] Sum of Square; [3] Degrees of Freedom; [4] Mean Square; [5] Significance Level.

For color removal, similar patterns were observed. Under fixed pH conditions (Table 4), the type of coagulant significantly affected color removal (F = 10.29, p = 0.001), while dosage again showed a weaker and statistically insignificant effect (F = 2.30, p = 0.088). When the variables were assessed under pH variation at optimal coagulant concentration (Table 5), the coagulant type remained the decisive factor with a high F-ratio of 18.27 (p < 0.001), while pH did not demonstrate a significant influence on color reduction (F = 1.39, p = 0.273).

These comprehensive ANOVA results (Tables 2–5) confirm that coagulant type is the most influential factor in determining both COD and color-removal efficiencies. Although dosage and pH can influence outcomes to some extent, their effects are considerably less significant unless paired correctly with an effective coagulant. This underscores the importance of strategic coagulant selection as a central element in optimizing treatment performance for complex wastewaters such as those from licorice-based pharmaceutical production.

Table 4. ANOVA of the significance of coagulant type and dose on Color at fixed pH.

SV [1]	SS [2]	Df [3]	MS [4]	F-Ratio	$F_{0.95}$	SL [5]
Coagulant Type	820,982	2	410,491	10.29	3.49	0.001
Error	798,164	20	39,908.2			
Total	1,619,146	22				
Coagulant Dose	614,780	5	122,956	2.3	2.77	0.088
Error	963,666	18	53,537			
Total	1,587,446	23				

[1] Source of Variation; [2] Sum of Square; [3] Degrees of Freedom; [4] Mean Square; [5] Significance Level.

Table 5. ANOVA, the significance of coagulant type and pH on Color (at optimal coagulant concentration).

SV [1]	SS [2]	Df [3]	MS [4]	F-Ratio	$F_{0.95}$	SL [5]
Coagulant (optimal concentration)	1,089,941	2	544,970.5	18.27	3.49	<0.001
Error	596,494.3	20	29,824.72			
Total	1,684,635	22				
pH	470,932.8	5	94,186.57	1.395	2.77	0.273
Error	1,215,503	18	67,527.91			
Total	1,684,635	23				

[1] Source of Variation; [2] Sum of Square; [3] Degrees of Freedom; [4] Mean Square; [5] Significance Level.

3.2. Identifying Optimal Coagulant

Parameters such as stirring speed, stirring and settling time were maintained steady across all cases, with only the coagulant dose being varied. For FC, the maximum removal rates achieved were 59.1% for COD and 34.13% for color at a dose of 800 mg L^{-1}. Using $Al_2(SO_4)_3$ as the coagulant, the peak removal percentages were 65.34% for COD and 36.32% for color, also at a dose of 800 mg L^{-1}. For PAC, removal rates of 61.1% for COD and 35.37% for color were attained at a dose of 1000 mg L^{-1}. Consequently, alum was designated as the coagulant for all subsequent experiments in this study. Figure 2 details the percentage reductions in COD and color achieved with each coagulant. It was observed that increasing the alum dose from 200 to 800 mg L^{-1} substantially improved the removal efficiencies of both COD and color, with the highest values in this experimental series reaching 65.34% for COD and 36.32% for color at 800 mg L^{-1}. However, further increasing the dose to 1000 mg L^{-1} resulted in negligible changes in removal efficiency for both responses.

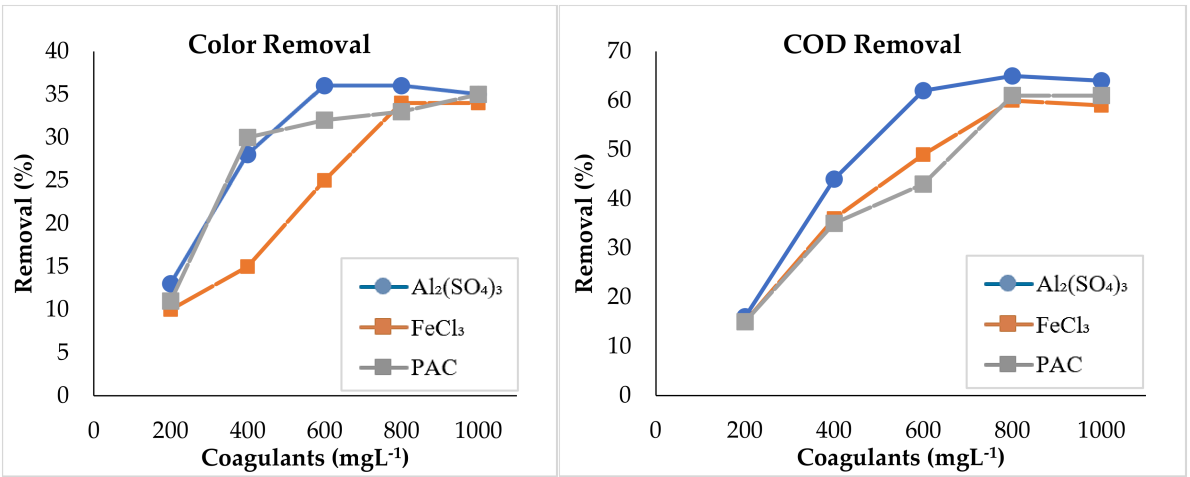


Figure 2. Impact of COD and color removal at varying doses, reported as applied salt/product dose and corresponding metal-equivalent dose where applicable, at pH 7, with a stirring speed of 40 rpm, stirring time of 20 min, and settling time of 30 min using $Al_2(SO_4)_3$, $FeCl_3$, and PAC.

At the optimum operating conditions, sludge generation was also evaluated as a critical operational parameter. Although high removal efficiency was achieved for COD, color removal remained the more persistent challenge, indicating the need for additional or complementary treatment in some cases. Despite variations in performance, the quantity of sludge produced remained relatively consistent across the different coagulants tested. A direct comparison of sludge volume at equal coagulant doses revealed that FC generated the largest amount of sludge, followed by PAC, while Al produced the lowest sludge volume, making it the most favorable option in terms of both efficiency and waste minimization. The physical appearance of the sludge varied with coagulant type: gray-white for alum, brown for PAC, and black for FC. The settleable solids content of the sludge ranged between 1 and 3%, consistent with typical coagulation processes. Sludge density was found to vary depending on the coagulant and dosage. FC produced the densest sludge, ranging between 800 and 860 mg L^{-1}, while alum generated the lowest-density sludge, approximately 600–640 mg L^{-1}. These findings align with previous research, which reported similar trends in sludge production and density under comparable treatment conditions [45,46]. The superior performance of alum can be explained by its coagulation mechanism, since $Al_2(SO_4)_3$ hydrolyses and forms aluminum hydroxide species and amorphous $Al(OH)_3$ precipitates. These species destabilize suspended and colloidal particles through charge neutralization, adsorption, and sweep flocculation. As a result, particulate organic matter, colloidal compounds, suspended solids, and part of the color-causing substances can be incorporated into settleable flocs. This mechanism explains the observed reduction in COD and color during the coagulation–flocculation stage.

3.3. Evaluating the ANN Model for Predicting Responses

The experimental treatment performance is expressed in terms of COD and color removal efficiencies calculated using Equation (1). In contrast, the two ANN output variables were residual COD and residual color. Accordingly, the subsequent GA optimization was formulated to minimize these residual responses, and the removal efficiencies reported under the optimum operating conditions were calculated from the corresponding residual values using Equation (1).

To create an optimal network, various structures were evaluated, including different numbers of neurons in the hidden layer, training algorithms, and activation functions. The network's performance during the training, validation, and testing stages was assessed based on the correlation coefficient (R) and error statistics such as mean absolute percentage error (MAPE) and normalized root mean square error (NRMSE). The results indicated that the optimal network, trained using the Levenberg–Marquardt (LM) algorithm, had 10 neurons in the hidden layer and used the tansig activation function. The mean errors in predicting the responses were 3.16% and 2.7%, with a correlation coefficient of 0.97 and 0.95 for residual COD and residual color respectively, which is very close to unity. Figure 3 depicts the learning process of the trained MLP predictive model, visualized by the MSE on both the training and validation sets.

Figure 4 features the identity line (dashed line) and the regression line (thick continuous line). A linear regression model applied to the data resulted in correlation coefficients of 0.98 for the training dataset, 0.95 for the test dataset, and 0.96 for the validation dataset for residual COD. Similarly, for residual color, the correlation coefficients were 0.99 for the training dataset, 0.81 for the test dataset, and 0.95 for the validation dataset. The comparison between the regression line and the identity line (1:1 line) at a significance level of 0.05 indicates that the differences in the slope and intercept are not significant. This demonstrates that the ANN model accurately predicts the responses in the treatment process. Additionally, Figure 5 shows the error histogram plot which the histogram is

reasonably centered on zero, confirming that the ANN model effectively represents the quality of the experimental region.

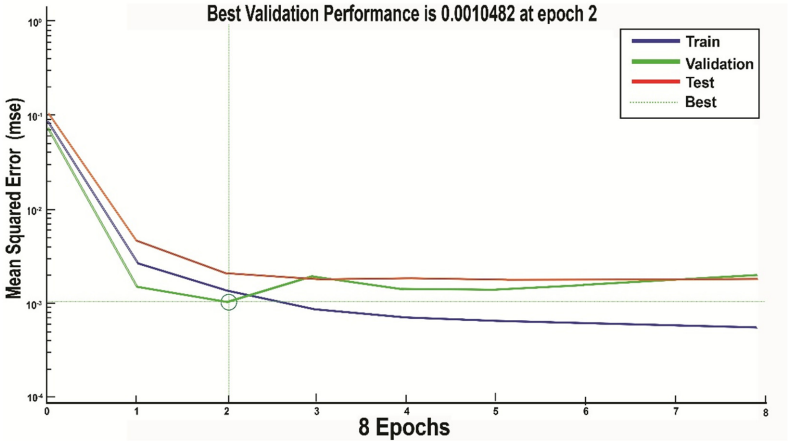


Figure 3. Mean squared error (MSE) performance of the ANN model during training, validation, and testing.

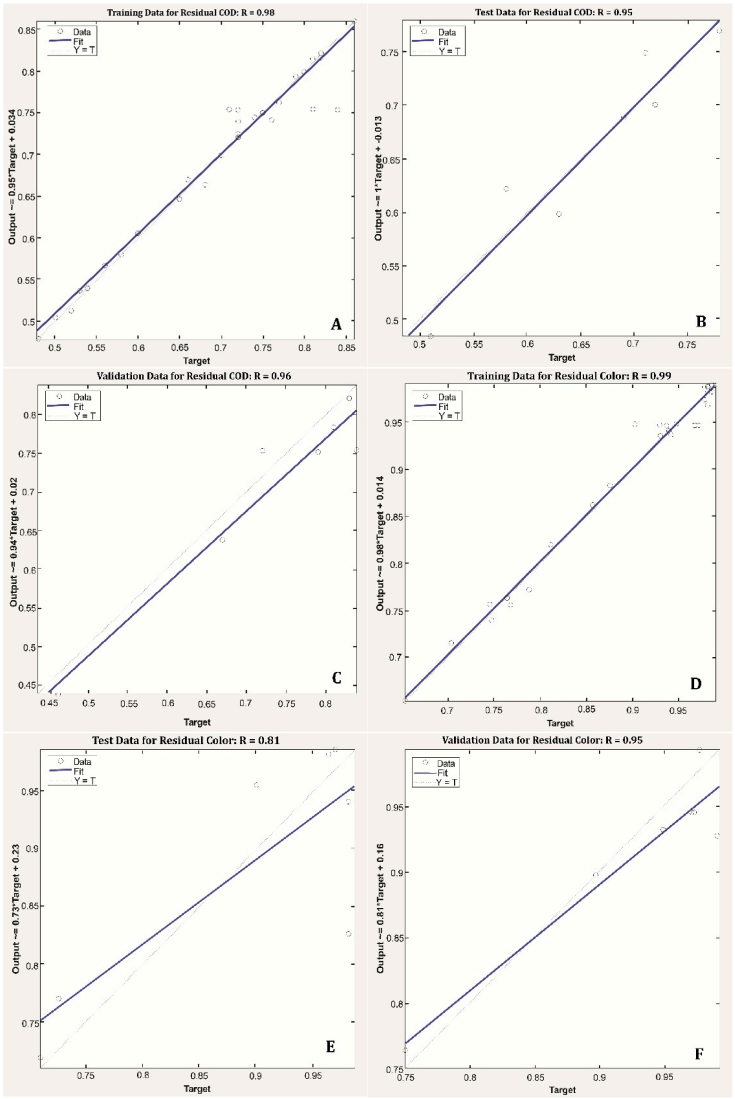


Figure 4. Training, test and validation curves (**A**–**C**) represent residual COD, and the row below (**D**–**F**) represents residual color of the developed ANN model. A total of 15% of points have been considered for the validation and 15% for the testing.

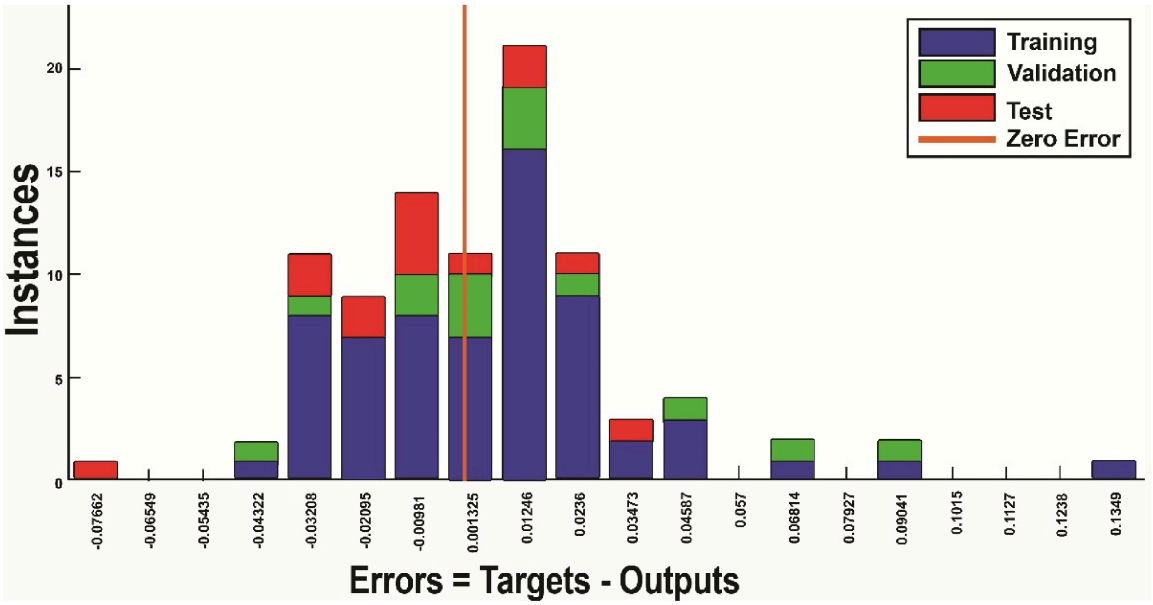


Figure 5. Error histogram plot.

3.4. Effect of Independent Variables

3.4.1. Effect of Dose

The first stage of treatment in this study employed $Al_2(SO_4)_3$ for coagulation. The maximum removal efficiencies achieved were 84.1% for COD and 49.5% for color at a dosage of 600 mg L^{-1} (Figure 6). It was observed that as the dosage increased from 200 mg L^{-1} to 600 mg L^{-1}, the removal efficiency increased from 38.2 to 49.5% for color and from 42.6 to 84.1% for COD removal. Nevertheless, when the dosage was further increased to 1000 mg L^{-1}, the removal efficiency for COD removal reduced, which can be attributed to several factors—neutralizing the negative charges on colloidal particles, allowing them to aggregate and settle. When the optimal dose is exceeded, the surface charge of the particles can become positive, leading to destabilization and reduced removal efficiency, and additionally, producing excessive sludge, hindering the settling process and potentially trapping some pollutants. The system can also reach a saturation point where additional coagulant does not contribute to further pollutant removal and may even result in diminishing returns. Furthermore, high doses of alum can lead to producing soluble aluminum complexes or precipitates, interfering with the coagulation process and reducing the efficiency of COD and color removal.

3.4.2. Impact of Ozonation Time

The data for COD and color removal efficiency at different pH levels and ozonation times shows a clear trend of increasing removal efficiency with both increasing pH and ozonation time (Figure 7). At pH 7, the color removal efficiency starts at 31.1% after 6 min and reaches 69.1% after 60 min. Similarly, at pH 12, the color removal efficiency increases from 48.2% to 90.7% over the same time. At lower pH levels, the color removal efficiency gradually improves with ozonation time. For instance, at pH 8, the removal efficiency increases from 40.1% at 6 min to 79.2% at 60 min. This indicates a moderate reaction rate where ozonation time plays a crucial role in enhancing the color removal efficiency. At pH 10, the color removal increases from 46.7% at 6 min to 89.3% at 60 min. Within the investigated ozonation-time series, the highest color-removal efficiency was observed at pH 11, reaching approximately 98% at around 40 min and remaining nearly constant with further ozonation time.

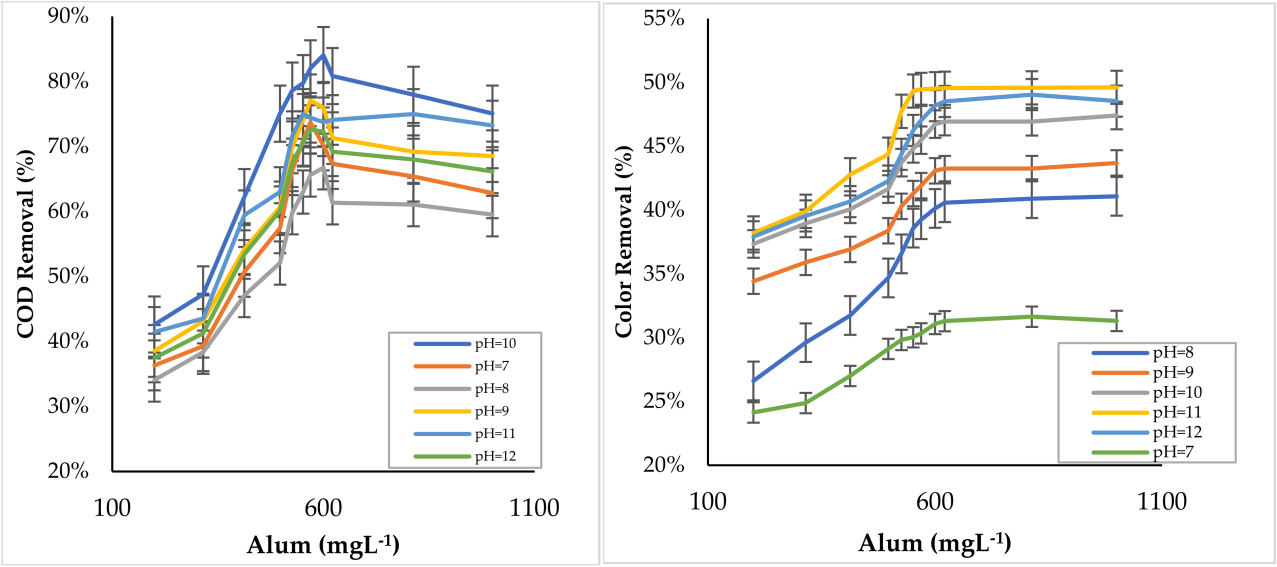


Figure 6. Impact of COD and color removal across various dosages with a stirring speed of 40 rpm, a stirring duration of 20 min, and a settling time of 30 min.

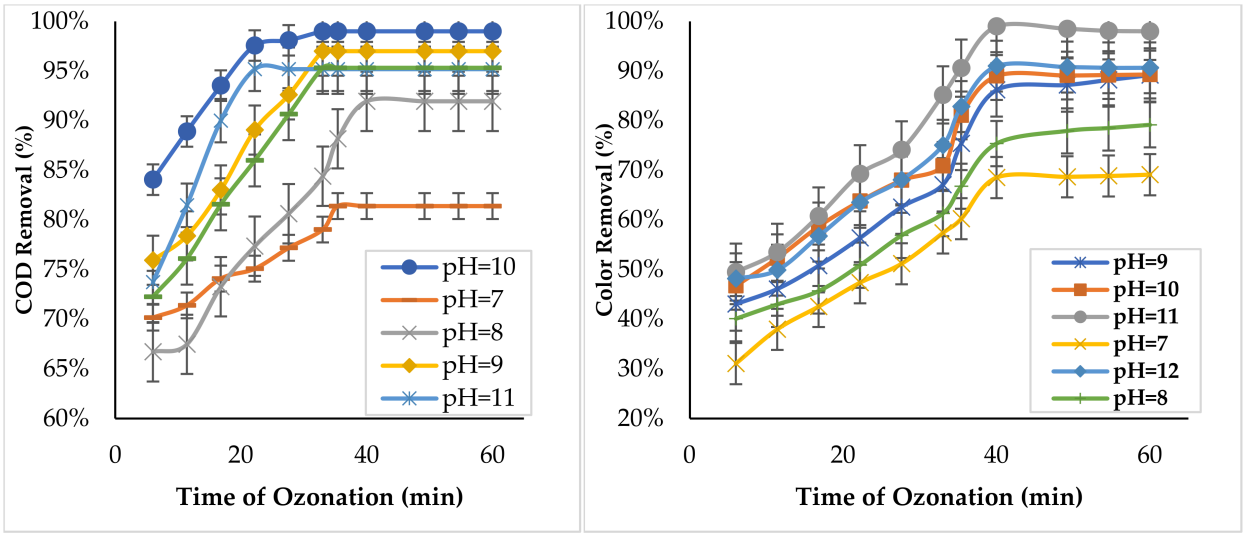


Figure 7. Effect of ozonation time and pH on COD and color removal.

The improvement in COD and color removal during ozonation can be attributed to both direct and indirect oxidation mechanisms. Molecular ozone directly reacts with electron-rich compounds such as phenolic structures, aromatic rings, and other chromophoric groups, contributing significantly to color removal, while its decomposition generates highly reactive hydroxyl radicals that can oxidize a broader range of organic pollutants. Under alkaline conditions, ozone decomposition is enhanced, increasing hydroxyl radical production and improving the degradation of refractory organic matter, which explains the higher removal efficiencies observed at elevated pH values. The plateau in removal efficiency at longer ozonation times suggests that the readily oxidizable compounds were removed during the initial stages, leaving more resistant intermediates and low-reactivity substances. Furthermore, wastewater constituents such as organic matter, carbonate/bicarbonate, chloride, bromide, and other ions may consume ozone and hydroxyl radicals through scavenging and secondary reactions, reducing the oxidants available for pollutant degradation. Therefore, the effectiveness of

ozonation depends not only on ozone dose and contact time but also on the composition of the wastewater matrix.

Furthermore, at pH 7, the COD removal efficiency starts at 70.2% after 6 min and reaches 81.4% after 60 min. At pH 12, the COD removal efficiency increases from 72.3% to 95.3% over the same time period. The COD removal efficiency at pH 8 improves from 66.7% at 6 min to 91.9% at 60 min, indicating a significant impact of ozonation time on the removal process. The trend is similar at pH 9, where the efficiency increases from 75.9% to 97%. Within the investigated ozonation-time series, COD removal at pH 10 increased from 84.1% at 6 min to approximately 99% at 33 min and remained nearly constant thereafter. High COD removal was also observed at pH 11 and pH 12 at longer ozonation times.

The results indicate that both pH and ozonation time significantly influence the removal efficiencies of COD and color. Higher pH levels generally result in higher removal efficiencies, which can be attributed to the enhanced formation of hydroxyl radicals in alkaline conditions, promoting more effective oxidation of organic compounds [47]. However, it is important to note that beyond certain ozonation times, the removal efficiencies for both COD and color tend to plateau, especially at higher pH levels [48]. This suggests that there is an optimal ozonation time after which additional ozonation does not significantly enhance removal efficiency, possibly due to the saturation of the oxidative capacity or the completion of the reaction processes. Similar results were achieved in a study on the ozonation of copper-mineral-processing wastewater, where the removal efficiency plateaued beyond a certain ozonation time, indicating the completion of reaction processes or saturation of the system's oxidative capacity [49].

3.5. GA-Optimization of the ANN Model

The multi-objective GA was applied to the trained ANN model by simultaneously minimizing the two ANN-predicted responses, namely residual COD and residual color. The optimization generated several candidate operating scenarios within the investigated parameter ranges. Among these solutions, the scenario providing the highest simultaneous removal of both COD and color was selected as the preferred operating condition.

$$Minimize\ (Responces) = \left(\sum_{j=1}^{10}\left[\frac{e^{\left(\sum_{i=1}^{3} w_{ji}x_i+b_j\right)} - e^{-\left(\sum_{i=1}^{3} w_{ji}x_i+b_j\right)}}{e^{\left(\sum_{i=1}^{3} w_{ji}x_i+b_j\right)} + e^{-\left(\sum_{i=1}^{3} w_{ji}x_i+b_j\right)}}\right] \times w_{2j}\right) + b \quad (7)$$

Equation (7) represents the ANN-based objective expression used for each predicted response. In the multi-objective optimization, the two objective functions were defined separately as the ANN-predicted residual COD and residual color and were minimized simultaneously.

$$\min_{x} F(x) = \begin{bmatrix} f_{COD}(x) \\ f_{Color}(x) \end{bmatrix} \quad (8)$$

where $f_{COD}(x)$ and $f_{Color}(x)$ represent the ANN-predicted residual COD and residual color, respectively, and x = [pH, D, t] where D is the alum dose and t is the ozonation time. The optimization was constrained to $7 \leq pH \leq 12$, $200 \leq D \leq 1000$ mg L^{-1} and $6 \leq t \leq 60$ min.

Among the candidate solutions generated by the multi-objective optimization, the operating condition providing the highest simultaneous removal of both COD and color was selected as the preferred optimum. This condition corresponded to pH 10, alum dose 610 mg L^{-1}, and ozonation time 53 min. Under these conditions, the ANN-predicted residual responses corresponded to approximately 98% COD removal and

99% color removal. Verification experiments showed removal efficiencies of approximately 98.1% ± 0.1 for both COD and color, closely matching the ANN-GA prediction (Figure 8).

In addition, TOC decreased from 3160 mg L^{-1} in the raw wastewater to 91.2 mg L^{-1} under the optimum treatment conditions, corresponding to approximately 97.1% TOC removal. This substantial decrease confirms a pronounced reduction in the organic carbon content of the wastewater following the combined coagulation–flocculation and ozonation treatment.

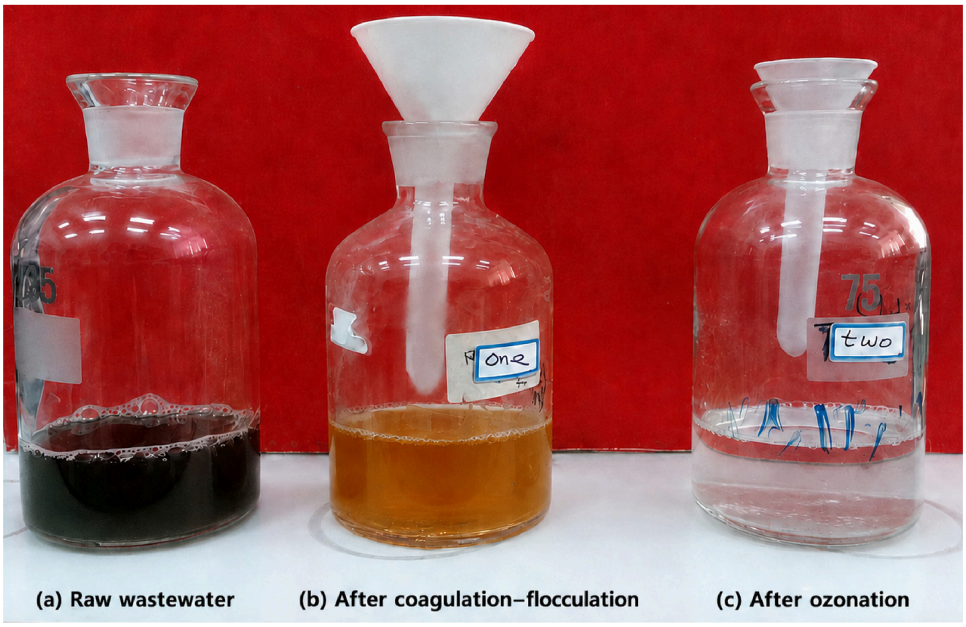


Figure 8. Visual comparison of wastewater samples at different treatment stages: (**a**) raw wastewater; (**b**) wastewater after coagulation–flocculation with alum (Phase I); and (**c**) wastewater after subsequent ozonation (Phase II).

The observation that COD removal was higher than color removal during the coagulation–flocculation step suggests that a substantial fraction of the oxidizable organic load was associated with particulate, colloidal, or easily destabilized matter that could be captured by floc formation and sedimentation. In contrast, part of the color-causing fraction may have consisted of more soluble or structurally stable chromophoric compounds that were not fully removed by coagulation alone. This behavior indicates that coagulation–flocculation mainly acted as a bulk removal and clarification step, while the subsequent ozonation stage was required to further degrade the more refractory color-imparting compounds.

3.6. Comparison with the Literature

Table 6 compares the treatment performance obtained in the present study with selected reports on wastewater treatment processes applied to similar or relevant industrial effluents. However, direct comparison among studies should be interpreted with caution because influent characteristics, target pollutants, reactor configurations, chemical inputs, and operating conditions differ considerably. Comparisons between coagulation-based systems, electrocoagulation, membrane processes, and hybrid advanced oxidation systems are not fully equivalent on a mechanistic or operational basis. Nevertheless, the present CF-OZ sequence demonstrated competitive COD and color removal at laboratory scale and may be considered a promising option for highly loaded licorice-processing wastewater. Future comparisons should include common performance indicators such as oxidant

dose, energy demand, sludge generation, and treatment cost to provide a more rigorous benchmarking basis.

Table 6. Comparison of various methods in similar research studies.

NO.	Type of Wastewater	Initial Wastewater Characteristics	Method Employed	Basic Experimental Conditions	Response Reduction	Reference
1	Licorice-processing wastewater Licorice-processing wastewater	COD: 1500–1600 mg L^{-1}; pH: 6.5; turbidity: 39–45 NTU; alkalinity: 230–285 mg $CaCO_3$ L^{-1}; conductivity: 450 µS cm^{-1}	Continuous electrocoagulation (EC) Continuous electrocoagulation (EC) with Fe rod electrodes	Fe electrodes; influent pH adjusted to 7; electrolysis time: 81.8 min; current density: 350 A m^{-2}; NaCl: 300 mg L^{-1}; mixing: 45 rpm	90.1% color, 89.4% COD, 82% turbidity, 73.3% alkalinity 94.6% color, 90.1% sCOD, 59.35% turbidity	[1]
2	Licorice-processing wastewater	COD: 6833 mg L^{-1}; BOD_5: 2956 mg L^{-1}; TSS: 748 mg L^{-1}; turbidity: 355 NTU; color: 3568 Pt-Co; pH: ~6.3	Hybrid biological (anaerobic–aerobic) and post-biological (lime–alum–ozone) WWTP	Full-scale, 105 m^3 d^{-1}; biological HRT: 8.2 d; alum: 0.05–0.08 g L^{-1}; lime: 0.05–0.10 g L^{-1}; settling: 15 h; ozone: 0.1 mg L^{-1} for 10 h	86–98% COD, 86–98% BOD_5, 86–98% TSS, phosphate, ammonium, nitrite, nitrate, turbidity; 68% color by biological treatment alone, 98% color with additional processes	[2]
3	Simulated licorice aqueous solution	Licorice feed concentration generally 0.1–0.5 g L^{-1}; commonly 0.3 g L^{-1}	Nanofiltration (NF) membranes (RPES-CPES)	Cross-flow filtration; transmembrane pressure: 6–12 bar; cross-flow velocity: 0.5–2.5 cm s^{-1}; filtration time generally 240 min	Enhanced permeability, antifouling capability, chemical resistance in acidic and basic environments	[50]
4	Licorice processing wastewater	High-strength model wastewater COD approximately 7000–8000 mg L^{-1}; $BOD_5/COD \approx 0.2$	Anaerobic digestion and activated sludge process	Batch anaerobic digestion followed by activated-sludge SBR; SBR HRT: 18–47 d; SRT: 47–97 d	15% COD reduction (anaerobic digestion); 80% COD reduction	[4]
5	Glycyrrhiza processing wastewater	pH: 4.55; conductivity: 1640 µS cm^{-1}; turbidity: 438 NTU; polysaccharides: 1.29 mg mL^{-1}; glycyrrhizic acid: 0.65 mg mL^{-1}; liquiritin: 0.15 mg mL^{-1}	Ultrasonic-assisted ultrafiltration combined with nanofiltration	MWCO 30 kDa, 500 W ultrasound, pH 5.0; Step 2: MWCO 10 kDa, 100 W, pH 8.0; Step 3: NF MWCO 800 Da, pH 8.0, two dilution/separation cycles	87.72% polysaccharide, 8.01% glycyrrhizic acid, 6.57% liquiritin rejection; Step 2: 40.65% glycyrrhizic acid and 9.22% liquiritin rejection; Step 3: 95.72% liquiritin and 3.70% total sugar rejection	[51]
This Study	Licorice processing wastewater	COD: 10,311 ± 407 mg L^{-1}; BOD: 4026 ± 29 mg L^{-1}; pH: 7.35 ± 0.11; turbidity: 749.8 ± 12.1 NTU; color: 1057.5 ± 23.8 mg Pt-CoL^{-1}; TDS: 8914 ± 30 mg L^{-1}; TSS: 745.4 ± 17.2 mg L^{-1}	Coagulation–flocculation plus ozonation	Batch sequential CF–OZ; pH: 10; alum: 610 mg L^{-1}; inlet O_3: 5 mg L^{-1}; gas flow: 10 L min^{-1}; ozonation time: 53 min	98% COD and color reduction	-

3.7. Limitations and Practical Implications

Although the integrated CF-OZ process achieved high COD and color removal efficiencies, several practical considerations remain for future work. First, the residual COD

after treatment indicates that post-treatment may still be required depending on the applicable discharge standard or reuse target. Second, no specific characterization of ozonation by-products was performed in the present study; therefore, the possible formation of intermediate oxidation products cannot be excluded, as ozonation can generate intermediate compounds and potentially harmful by-products, depending on wastewater composition and reaction conditions. Although the inlet ozone concentration and gas flow rate were measured and controlled during the experiments, dissolved ozone and residual ozone in the off-gas were not quantitatively monitored because the present study focused primarily on treatment performance. Consequently, the actual transferred and consumed ozone dose could not be determined, which represents a limitation of the present study. Third, large-scale application would require more detailed assessment of ozone consumption, off-gas handling, energy demand, sludge production, and overall operating cost. Moreover, sludge generation and management should also be considered in future scale-up assessments, particularly in relation to sludge volume, dewaterability, disposal requirements, and associated operating costs. Therefore, the present results should be interpreted as a laboratory-scale feasibility and optimization assessment rather than a complete process validation for industrial implementation. Lastly, although alum achieved the highest removal efficiency, the resulting sludge would still require treatment and disposal. In addition, operation at pH 10 may require both pH adjustment and subsequent neutralization. The ozonation step is also expected to contribute significantly to energy demand. Future studies should evaluate ozone consumption, energy requirements, sludge production, and overall treatment cost.

3.8. Recommendation for Further Studies

Future studies should extend the analytical assessment of licorice wastewater treatment beyond the conventional physicochemical parameters considered in the present work. In particular, chromatographic techniques such as HPLC or GC–MS are recommended to identify major organic compounds and possible transformation products before and after treatment. Toxicity assays should also be incorporated to evaluate whether the treated effluent presents any residual ecological effects. In addition, further investigation of ozonation by-products and the fate of specific licorice-derived compounds would provide a more comprehensive understanding of the treatment mechanisms and environmental safety of the combined coagulation–flocculation and ozonation process.

4. Conclusions

The combination of coagulation–flocculation followed by ozone oxidation was employed to treat licorice-processing wastewater. The optimal configuration of the ANN features a tansig activation function, utilizes the LM training algorithm, and includes 10 neurons in the hidden layer. Statistical analyses confirm minimal variance between observed and predicted data, underscoring the model's robust predictive accuracy. Subsequently, a multi-objective GA was coupled with the trained ANN model to simultaneously minimize residual COD and residual color. From the generated candidate solutions, the operating condition providing the highest simultaneous COD and color removal was selected as the preferred optimum, corresponding to approximately 98% COD removal and 99% color removal at pH 10, an alum dose of 610 mg L^{-1}, and an ozonation time of 53 min, while TOC removal under the same optimized condition reached approximately 97.1%. Importantly, ANOVA results highlighted that the type of coagulant was the most statistically significant factor influencing treatment efficiency ($p < 0.01$), while pH and dosage showed comparatively lower effects unless used under optimal conditions. These

findings reinforce the need for careful selection of coagulant type during process design. Compared with existing treatment approaches reported in the literature, the integrated CF–OZ process, supported by ANN–GA modeling and statistical analysis, provides a promising laboratory-scale approach for reducing organic load and color in licorice-based pharmaceutical wastewater and warrants further evaluation for potential scale-up. Moreover, this approach offers a valuable framework for future studies targeting complex industrial effluents.

Author Contributions: Conceptualization, B.R.B. and A.K.-J.; methodology, B.R.B. and A.K.-J.; software, B.R.B.; validation, B.R.B. and A.K.-J.; formal analysis, B.R.B.; investigation, B.R.B.; resources, A.K.-J.; data curation, B.R.B.; writing—original draft preparation, B.R.B.; writing—review and editing, B.R.B. and A.K.-J.; visualization, B.R.B.; supervision, A.K.-J.; project administration, A.K.-J.; funding acquisition, A.K.-J. All authors have read and agreed to the published version of the manuscript.

Funding: This research received no external funding. City University Qatar supported the APC payment.

Data Availability Statement: The data presented in this study are available within the article. Further information or additional supporting data can be obtained from the corresponding author upon reasonable request.

Conflicts of Interest: The authors declare no conflicts of interest.

Abbreviations

The following abbreviations are used in this manuscript:

PAC	Polyaluminum Chloride
FC	Ferric Chloride
COD	Chemical Oxygen Demand
ANOVA	Analysis of Variance
BOD	Biochemical Oxygen Demand
TDS	Total Dissolved Solids
TSS	Total Suspended Solids
MLP	Multilayer Perceptron
ANN	Artificial Neural Network

References

1. Abbasi, S.; Mirghorayshi, M.; Zinadini, S.; Zinatizadeh, A. A novel single continuous electrocoagulation process for treatment of licorice processing wastewater: Optimization of operating factors using RSM. *Process Saf. Environ. Prot.* **2020**, *134*, 323–332. [CrossRef]
2. Houshyar, E.; Bacenetti, J. Development of a full-scale wastewater treatment plant for licorice root processing factories: A hybrid biodegradation-lime-alum-ozonation process. *Sci. Total Environ.* **2023**, *893*, 164688. [CrossRef] [PubMed]
3. Hartal, O.; Madinzi, A.; Rifi, S.K.; Haddaji, C.; Kurniawan, T.A.; Anouzla, A.; Souabi, S. Optimization of coagulation-flocculation process for wastewater treatment from vegetable oil refineries using chitosan as a natural flocculant. *Environ. Nanotechnol. Monit. Manag.* **2024**, *22*, 100957. [CrossRef]
4. Ramaswami, S.; Behrendt, J.; Otterpohl, H.G.a.R. Pretreatment of Wastewater from Licorice Processing—A Preliminary Evaluation. *Water Environ. Res.* **2016**, *88*, 2032–2039. [CrossRef] [PubMed]
5. Mouhri, G.E.; Elmansouri, I.; Amakdouf, H.; Belhassan, H.; Kachkoul, R.; Oumari, F.E.E.; Merzouki, M.; Lahrichi, A. Evaluating the effectiveness of coagulation–flocculation treatment on a wastewater from the moroccan leather tanning industry: An ecological approach. *Heliyon* **2024**, *10*, e27056. [CrossRef] [PubMed]
6. Chik, C.E.N.C.E.; Kurniawan, S.B.; Shukri, Z.N.A.; Terkula, I.B.; Wahab, F.; Endut, A.; Lananan, F.; Hasan, H.A.; Abdullah, S.R.S.; Kasan, N.A. Chitosan coagulant: Coagulation/flocculation studies on turbidity removal from aquaculture wastewater by response surface methodology. *Int. J. Environ. Sci. Technol.* **2023**, *21*, 805–816. [CrossRef]
7. Liao, Y.; Wang, L.; Tian, Y.; Li, J.; Zhou, Q.; Li, A.; Hua, M.; Pan, Y. Effects of ozonation-enhanced coagulation on effluent organic matter and disinfection byproducts. *J. Clean. Prod.* **2025**, *490*, 144801. [CrossRef]

8. Marques, D.G.; De Melo Franco Domingos, J.; Nolasco, M.A.; Campos, V. Textile effluent treatment using coagulation-flocculation and a hydrodynamic cavitation reactor associated with ozonation. *Chem. Eng. Sci.* **2024**, *304*, 121094. [CrossRef]
9. Conidi, C.; Fucà, L.; Drioli, E.; Cassano, A. A Membrane-Based Process for the Recovery of Glycyrrhizin and Phenolic Compounds from Licorice Wastewaters. *Molecules* **2019**, *24*, 2279. [CrossRef] [PubMed]
10. Haddaji, C.; Rifi, S.K.; Digua, K.; Madinzi, A.; Chatoui, M.; Driouich, A.; Ettaloui, Z.; Kurniawan, T.A.; Anouzla, A.; Souabi, S. Optimization of the coagulation-flocculation process using response surface methodology for wastewater pretreatment generated by vegetable oil refineries: A path towards environmental sustainability. *Environ. Nanotechnol. Monit. Manag.* **2024**, *22*, 100973. [CrossRef]
11. Aziz, A.; Basheer, F.; Sengar, A.; Irfanullah, N.; Khan, S.U.; Farooqi, I.H. Biological wastewater treatment (anaerobic-aerobic) technologies for safe discharge of treated slaughterhouse and meat processing wastewater. *Sci. Total Environ.* **2019**, *686*, 681–708. [CrossRef] [PubMed]
12. Di Trapani, D.; Corsino, S.F.; Torregrossa, M.; Viviani, G. Treatment of high strength industrial wastewater with membrane bioreactors for water reuse: Effect of pre-treatment with aerobic granular sludge on system performance and fouling tendency. *J. Water Process Eng.* **2019**, *31*, 100859. [CrossRef]
13. Louhichi, G.; Khouni, A.E.; Ghrabi, A.; Khouni, I. Phytotoxicity assessment of treated vegetable oily wastewater via environmentally coagulation/flocculation and membrane filtration technologies using lettuce (*Lactuca sativa*) seeds. *Environ. Sci. Pollut. Res.* **2024**, *31*, 57204–57228. [CrossRef] [PubMed]
14. Shoukat, R.; Khan, S.J.; Jamal, Y. Hybrid anaerobic-aerobic biological treatment for real textile wastewater. *J. Water Process Eng.* **2019**, *29*, 100804. [CrossRef]
15. Zangeneh, H.; Zinatizadeh, A.; Feyzi, M.; Zinadini, S.; Bahnemann, D. Application of a novel triple metal-nonmetal doped TiO_2 (K-B-N-TiO_2) for photocatalytic degradation of Linear Alkyl Benzene (LAB) industrial wastewater under visible light. *Mater. Sci. Semicond. Process.* **2018**, *75*, 193–205. [CrossRef]
16. Sardari, K.; Askegaard, J.; Chiao, Y.; Darvishmanesh, S.; Kamaz, M.; Wickramasinghe, S.R. Electrocoagulation followed by ultrafiltration for treating poultry processing wastewater. *J. Environ. Chem. Eng.* **2018**, *6*, 4937–4944. [CrossRef]
17. Zourif, A.; Kouniba, S.; Guendouzi, M.E. Valorization of palm petiole waste as natural biocoagulants: Optimizing coagulation-flocculation for sustainable wastewater treatment and advancing circular economy in agriculture. *Biocatal. Agric. Biotechnol.* **2024**, *63*, 103473. [CrossRef]
18. Can-Güven, E.; Bayat, M.E.; Guvenc, S.Y.; Varank, G. Refractory pollutants removal from industrial wastewater by a coupled process of coagulation-flocculation and alternative electrochemical advanced oxidation processes. *Colloids Surf. A Physicochem. Eng. Asp.* **2024**, *707*, 135916. [CrossRef]
19. Costa, F.C.; Moreira, V.R.; Guimarães, R.N.; Moser, P.B.; Santos, L.V.; De Paula, E.C.; Amaral, M.C. Pre-oxidation and coagulation-flocculation as a pretreatment to UF-RO applied for surface water treatment and arsenic removal. *Desalination* **2024**, *586*, 117855. [CrossRef]
20. Dobrosz-Gómez, I.; Quintero-Arias, J.; Gómez-García, M. Coagulation-Flocculation—Fenton-Neutralization sequential process for the treatment of industrial effluent polluted with AB194 dye. *Case Stud. Chem. Environ. Eng.* **2024**, *9*, 100720. [CrossRef]
21. Tahraoui, H.; Toumi, S.; Boudoukhani, M.; Touzout, N.; Sid, A.N.E.H.; Amrane, A.; Belhadj, A.; Hadjadj, M.; Laichi, Y.; Aboumustapha, M.; et al. Evaluating the effectiveness of Coagulation–Flocculation treatment using aluminum sulfate on a polluted Surface Water source: A Year-Long Study. *Water* **2024**, *16*, 400. [CrossRef]
22. Thuan, N.C.; Phat, V.V.; Hang, T.T.T.; Luu, T.L.; Tripple, J.; Wagner, M. Treatment of seafood processing wastewater toward carbon neutrality: A comparison between coagulation/flocculation, chemical oxidation and absorbent methods. *Case Stud. Chem. Environ. Eng.* **2024**, *10*, 100792. [CrossRef]
23. Zhao, C.; Zhou, J.; Yan, Y.; Yang, L.; Xing, G.; Li, H.; Wu, P.; Wang, M.; Zheng, H. Application of coagulation/flocculation in oily wastewater treatment: A review. *Sci. Total Environ.* **2021**, *765*, 142795. [CrossRef] [PubMed]
24. Belkodia, K.; Mersly, L.E.; Edaala, M.; Achtak, H.; Tahiri, A.A.; Briche, S.; Rafqah, S. Cheese wastewater treatment through combined coagulation-flocculation and photo-Fenton-like advanced oxidation processes for reuse in irrigation: Effect of operational parameters and phytotoxicity assessment. *Environ. Sci. Pollut. Res.* **2024**, *31*, 11801–11814. [CrossRef] [PubMed]
25. Pinedo, M.L.; Riascos, B.D.; Quintero, X.E.; Costa, C. Mechanism of pH sensitive flocculation for organic load and colour reduction in landfill leachate. *Waste Manag.* **2022**, *144*, 163–172. [CrossRef] [PubMed]
26. Achite, M.; Farzin, S.; Elshaboury, N.; Anaraki, M.V.; Amamra, M.; Toubal, A.K. Modeling the optimal dosage of coagulants in water treatment plants using various machine learning models. *Environ. Dev. Sustain.* **2022**, *26*, 3395–3421. [CrossRef]
27. Dostiyev, H.; Gönder, Z.B. A comparative investigation of chemical coagulation and electrocoagulation for the post-treatment of confectionery wastewater. *Int. J. Environ. Sci. Technol.* **2023**, *21*, 3661–3674. [CrossRef]
28. Enfiyeci, A.; Çifçi, D.İ. Comparison of coagulation–Fenton oxidation and coagulation–adsorption processes in textile and chemical industry mixed wastewater. *J. Chem. Technol. Biotechnol.* **2025**, *100*, 466–476. [CrossRef]

29. Kang, Y.; Wang, J.; Li, Z. Enhancing pollutants removal in hospital wastewater: Comparative analysis of PAC coagulation vs. bio-contact oxidation, highlighting the impact of outdated treatment plants. *J. Hazard. Mater.* **2024**, *471*, 134340. [CrossRef] [PubMed]
30. Choque-Quispe, Y.; Solano-Reynoso, A.M.; Dueñas-Valcarcel, C.E.; Arostegui-Leon, E.; Rodriguez-Cardenas, L.; Choque-Quispe, D. Application of Nostoc sphaericum and Opuntia ficus-indica Mucilage in the Coagulation–Flocculation Process of Sanitary Landfill Leachate: An Optimization Study. *Polymers* **2026**, *18*, 474. [CrossRef] [PubMed]
31. Noor, M.H.M.; Harith, M.H.A.; Razmi, F.A.; Ngadi, N.; Othman, Q.A. Big picture on coagulation-flocculation technology integrated artificial intelligence for wastewater treatment application: A systematic mapping review. *Process Saf. Environ. Prot.* **2026**, *207*, 108445. [CrossRef]
32. Matheri, A.N.; Ntuli, F.; Ngila, J.C.; Seodigeng, T.; Zvinowanda, C. Performance prediction of trace metals and cod in wastewater treatment using artificial neural network. *Comput. Chem. Eng.* **2021**, *149*, 107308. [CrossRef]
33. Mesutoğlu, Ö.Ç.; Gök, O. Prediction of COD in industrial wastewater treatment plant using an artificial neural network. *Sci. Rep.* **2024**, *14*, 13750. [CrossRef] [PubMed]
34. Warren-Vega, W.M.; Montes-Pena, K.D.; Romero-Cano, L.A.; Zarate-Guzman, A.I. Development of an artificial neural network (ANN) for the prediction of a pilot scale mobile wastewater treatment plant performance. *J. Environ. Manag.* **2024**, *366*, 121612. [CrossRef] [PubMed]
35. Broujeni, B.R.; Nilchi, A.; Azadi, F. Adsorption modeling and optimization of thorium (IV) ion from aqueous solution using chitosan/TiO_2 nanocomposite: Application of artificial neural network and genetic algorithm. *Environ. Nanotechnol. Monit. Manag.* **2021**, *15*, 100400. [CrossRef]
36. Palma, D.; Antela, K.U.; Prevot, A.B.; Cervera, M.L.; Morales-Rubio, A.; Sáez-Hernández, R. Artificial neural networks applied to photo-Fenton process: An innovative approach to wastewater treatment. *Water Sci. Eng.* **2025**, *18*, 324–334. [CrossRef]
37. Biswas, P.P.; Chen, W.; Lam, S.S.; Park, Y.; Chang, J.; Hoang, A.T. A comprehensive study of artificial neural network for sensitivity analysis and hazardous elements sorption predictions via bone char for wastewater treatment. *J. Hazard. Mater.* **2024**, *465*, 133154. [CrossRef] [PubMed]
38. Azadi, S.; Karimi-Jashni, A.; Javadpour, S. Photocatalytic treatment of landfill leachate using W-Doped TiO_2 nanoparticles. *J. Environ. Eng.* **2017**, *143*, 04017049. [CrossRef]
39. Mandal, S.; Mahapatra, S.; Patel, R. Enhanced removal of Cr(VI) by cerium oxide polyaniline composite: Optimization and modeling approach using response surface methodology and artificial neural networks. *J. Environ. Chem. Eng.* **2015**, *3*, 870–885. [CrossRef]
40. Mohan, S.; Singh, Y.; Verma, D.K.; Hasan, S.H. Synthesis of CuO nanoparticles through green route using Citrus limon juice and its application as nanosorbent for Cr(VI) remediation: Process optimization with RSM and ANN-GA based model. *Process Saf. Environ. Prot.* **2015**, *96*, 156–166. [CrossRef]
41. Clesceri, L.S.; Greenberg, A.E.; Eaton, A.D. (Eds.) *Standard Methods for the Examination of Water and Wastewater*, 20th ed.; American Public Health Association: Washington, DC, USA; American Water Works Association: Denver, CO, USA; Water Environment Federation: Alexandria, VA, USA, 1998.
42. Puri, A.; Kumar, M. A review of permissible limits of drinking water. *Indian J. Occup. Environ. Med.* **2012**, *16*, 40. [CrossRef] [PubMed]
43. Mahmoodi, N.M.; Oveisi, M.; Taghizadeh, A.; Taghizadeh, M. Novel magnetic amine functionalized carbon nanotube/metal-organic framework nanocomposites: From green ultrasound-assisted synthesis to detailed selective pollutant removal modelling from binary systems. *J. Hazard. Mater.* **2019**, *368*, 746–759. [CrossRef] [PubMed]
44. Salehi, I.; Shirani, M.; Semnani, A.; Hassani, M.; Habibollahi, S. Comparative study between response surface methodology and artificial neural network for adsorption of crystal violet on magnetic activated carbon. *Arab. J. Sci. Eng.* **2016**, *41*, 2611–2621. [CrossRef]
45. Balik, Ö.Y.; Aydin, S. Coagulation/flocculation optimization and sludge production for pre-treatment of paint industry wastewater. *Desalin. Water Treat.* **2015**, *57*, 12692–12699. [CrossRef]
46. Teutli-León, M.; Pérez-López, M.E. Sludge density prediction in a wastewater chemical coagulation process. *J. Water Resour. Prot.* **2013**, *5*, 1–4. [CrossRef]
47. Zhao, M.; Wang, X.; Wang, S.; Gao, M. Hydroxyl radical induced Cr flocculation via redox reaction: The extending application of heterogeneous advanced oxidation processes on Cr removal. *J. Hazard. Mater.* **2023**, *452*, 131282. [CrossRef] [PubMed]
48. Mir, I.S.; Riaz, A.; Roy, J.S.; Fréchette, J.; Morency, S.; Gomes, O.P.; Dumée, L.F.; Greener, J.; Messaddeq, Y. Removal of cadmium and chromium heavy metals from aqueous medium using composite bacterial cellulose membrane. *Chem. Eng. J.* **2024**, *490*, 151665. [CrossRef]
49. Kulišťáková, A. Removal of pharmaceutical micropollutants from real wastewater matrices by means of photochemical advanced oxidation processes—A review. *J. Water Process Eng.* **2023**, *53*, 103727. [CrossRef]

50. Oulad, F.; Zinadini, S.; Zinatizadeh, A.A.; Derakhshan, A.A. Preparation and characterization of high permeance functionalized nanofiltration membranes with antifouling properties by using diazotization route and potential application for licorice wastewater treatment. *Sep. Purif. Technol.* **2022**, *280*, 119639. [CrossRef]
51. Li, C.; Ma, Y.; Tang, S.; Xu, Y.; Shen, X.; Qiu, R.; Cai, S.; Ma, Y.; Zhi, X. Ultrasonic-assisted membrane processes for the systematic purification of glycyrrhiza wastewater. *Ultrason. Sonochem.* **2024**, *111*, 107098. [CrossRef] [PubMed]

Disclaimer/Publisher's Note: The statements, opinions and data contained in all publications are solely those of the individual author(s) and contributor(s) and not of MDPI and/or the editor(s). MDPI and/or the editor(s) disclaim responsibility for any injury to people or property resulting from any ideas, methods, instructions or products referred to in the content.